Asian Journal of Pharmaceutical Sciences 16 (2021) 337–349

Available online at www.sciencedirect.com

ScienceDirect

journal homepage: www.elsevier.com/locate/AJPS

Original Research Paper

Small changes in the length of diselenide bond-containing linkages exert great influences on the antitumor activity of docetaxel homodimeric prodrug nanoassemblies

Lingxiao Li, Shiyi Zuo, Fudan Dong, Tian Liu, Yanlin Gao, Yinxian Yang, Xin Wang, Jin Sun, Bingjun Sun, Zhonggui He**

Department of Pharmaceutics, Wuya College of Innovation, Shenyang Pharmaceutical University, Shenyang 110016, China

ARTICLE INFO

Article history:
Received 30 December 2020
Revised 19 February 2021
Accepted 21 February 2021
Available online 25 February 2021

Keywords:
Diselenide bond
Homodimeric prodrug
Docetaxel
Self-assembly
Redox responsive

ABSTRACT

Homodimeric prodrug-based self-assembled nanoparticles, with carrier-free structure and ultrahigh drug loading, is drawing more and more attentions. Homodimeric prodrugs are composed of two drug molecules and a pivotal linkage. The influence of the linkages on the self-assembly, *in vivo* fate and antitumor activity of homodimeric prodrugs is the focus of research. Herein, three docetaxel (DTX) homodimeric prodrugs are developed using different lengths of diselenide bond-containing linkages. Interestingly, compared with the other two linkages, the longest diselenide bond-containing linkage could facilitate the self-delivery of DTX prodrugs, thus improving the stability, circulation time and tumor targeting of prodrug nanoassemblies. Besides, the extension of linkages reduces the redox-triggered drug release and cytotoxicity of prodrug nanoassemblies in tumor cells. Although the longest diselenide bond-containing prodrug nanoassemblies possessed the lowest cytotoxicity to 4T1 cells, their stable nanostructure maintained intact during circulation and achieve the maximum accumulation of DTX in tumor cells, which finally "turned the table". Our study illustrates the crucial role of linkages in homodimeric prodrugs, and gives valuable proposal for the development of advanced nano-DDS for cancer treatment.

1. Introduction

Despite drug therapy has many drawbacks such as restricted efficacy, narrow therapeutic window and off-set toxicity, it still remains one of the most powerful strategy in cancer therapy [1]. For example, docetaxel (DTX), a well-known taxane-containing antitumor drug, is widely applied for the treatment of breast cancer, ovarian cancer and lung cancer, etc. [2]. Notably, it is also used as a main component of the neoadjuvant therapy for the advanced triple-negative breast cancer (TNBC) [3–5]. However, the administration of DTX

* Corresponding authors.
E-mail addresses: sunbingjun_spy@sina.com (B.J. Sun), hezhgui_student@aliyun.com (Z.G. He).
Peer review under responsibility of Shenyang Pharmaceutical University.

https://doi.org/10.1016/j.ajps.2021.02.002

always give rise to serious neutropenia and neurotoxicity [6,7]. In addition, as DTX is poorly soluble in water, the clinical formulation (Taxotere®) has to use non-ionic surfactant Tween 80 and ethanol as solubilizers, which could induce undesirable hypersensitivity reactions [8]. Even with the help of solubilizers, Taxotere® has poor stability and tend to precipitate after dilution. All these drawbacks restrict the clinical application of DTX [9]. Rational design of advanced drug delivery systems (DDS) for efficient cancer therapy is still a challenge.

To address these problems, prodrug strategies have been emerged to improve the undesirable properties of anticancer drugs in terms of solubility, stability, and tumor-selectivity [10–12]. In addition, nanoparticulate drug delivery systems (nano-DDSs) are also widely investigated to improve the circulation time and tumor-targeting of anticancer drugs [12–17]. Moreover, prodrug nanoassemblies, which combining the benefits of nanomedicine and prodrug strategies, is drawing more and more attentions in recent years [18–20]. Particularly, homodimeric prodrugs are developed by bridging two drug molecules together using a special linkage. Because the prodrugs can play the dual role of goods and carriers, the homodimeric prodrug nanoassemblies possess ultrahigh drug loading (even over 60%, w/w) [21]. In addition, prodrug nanoassemblies avoid the use of bioincompatible solubilizers, which would help to improve the medication safety and patient compliance [22].

It has been founded that the central linkages have great impacts on the self-assembly, drug release, *in vivo* fate, and antitumor activity of prodrugs [21]. In our previous studies, six paclitaxel-citronellol monomeric prodrugs were synthesized using thioether bond, disulfide bond, selenoether bond, diselenide bond, carbon bond and dicarbide bond as linkages [19]. Diselenide bond-containing linkage, with distinct bond angle and dihedral angle, could promote the self-assembly of paclitaxel-citronellol monomeric prodrugs. Additionally, diselenide bond exhibited redox dual-responsivity, leading to rapid drug release in the redox-heterogeneous microenvironment of tumor cells [20,23–29]. We also found that diselenide bond was a promising candidate for the design of docetaxel homodimeric prodrug nanoassemblies compared with disulfide and dicarbide bond [20]. Furthermore, the length of disulfide bond-containing linkages played a key role in the antitumor activity of paclitaxel-citronellol monomeric prodrug nanoassemblies [30]. Compared with monomeric prodrugs, the rigid chemical structure of homodimeric prodrugs often limit their self-assembly ability, and the drug release mechanism are also different [31–33]. Therefore, we speculate that the length of diselenide bond-containing linkages maybe have certain impacts on homodimeric prodrug nanoassemblies. However, no related work has been reported to our knowledge.

Herein, three DTX homodimeric prodrugs were designed and synthesized via different lengths of diselenide bond-containing linkages. The prodrugs were defined as α-DSeSeD, β-DSeSeD and γ-DSeSeD, since the selenium atom was situated at the α-, β-, or γ-position of the carbonyl group, respectively (Fig. 1). All three prodrugs could form nanoassemblies with ultrahigh drug loading (~70%, w/w). Interestingly, the length of the diselenide bond-containing linkages not only affected the self-assembly ability, but also impacted the redox-responsive drug release, thereby influencing the stability, pharmacokinetics, biodistribution and cytotoxicity of prodrug nanoassemblies. Moreover, the relationships between the linkages and the anticancer efficacy of prodrug nanoassemblies were also investigated in details.

2. Materials and methods

2.1. Materials and reagent

DiR, Docetaxel and glutathione (GSH) were provided by Meilun Biotech (Dalian, China). Bromoacetic acid, selenium, 1-ethyl-3-(3-dimethyllaminopropyl) carbodiimide hydrochloride (EDCI), 3-bromopropionic acid, sodium borohydride ($NaBH_4$), 4-dimethylaminopyrideine (DMAP), Hydrogen peroxide (H_2O_2), 4-bromobutyric acid and coumarin-6 were all supplied by Aladdin (Shanghai, China). 2-distearoyl-sn-glycerol-3-phosphoethanolamine-N-methyl (polyethylene glycol)−2000 (DSPE-PEG_{2k}) were obtained from Shanghai Advanced Vehicle Technology Pharmaceutical Ltd. (Shanghai, China). Fetal bovine serum (FBS) was supplied by Hyclone (Beijing, China). Trypsin and 3-(4,5-dimethylthiazol-2-yl)−2,5-diphenyltetrazolium bromide (MTT) were obtained from Gibco (Beijing, China). The other reagents mentioned in this work were of analytical or HPLC grade.

2.2. Synthesis of diacid linkers

The synthesizing method of diselenide linkers was similar to our previous study [20]. Briefly, selenium powder (1.58 g, 20 mmol) was added to a flask, and then pure water was added. Under nitrogen atmosphere, $NaBH_4$ (1.51 g, 40 mmol) solution was added dropwise into the above system, and then violently stirred at 0 °C. After the solution became clear, additional selenium powder (1.58 g, 20 mmol) was added, and the reaction mixture was heated up to 110 °C for 30 min until a dark brownish-red solution was gained. The bromoacetic acid (5.56 g, 40 mmol) aqueous solution was added dropwise to the mixture, and stirred at 25 °C for 12 h. After that, filtration was utilized to remove impurities of reaction mixture, and the pH of the filtrate was regulated to 3.0–4.0 using diluted hydrochloric acid. Then ethyl acetate was used to extract the supernatant. After 3 times extraction, the ethyl acetate layer was dried, filtered, and removed by reduced pressure distillation to gain the target product 2, 2′-diselenobisdiglycolic acid (25% yield).

Synthesis of 3, 3′-diselenobisdipropionic acid and 4, 4′-diselenobisdibutyric acid were similar to 2, 2′-diselenobisdiglycolic acid, which replace the bromoacetic acid to 3-bromopropionic acid (6.12 g, 40 mmol) and 4-bromobutyric acid (6.68 g, 40 mmol) respectively (20%−30% yield).

2.3. Synthesis of DTX homodimeric prodrugs

Three DTX homodimeric prodrugs were synthesized as previously reported with few modifications [20]. Briefly, DTX (646.32 mg, 0.8 mmol) and diacid linker (2,

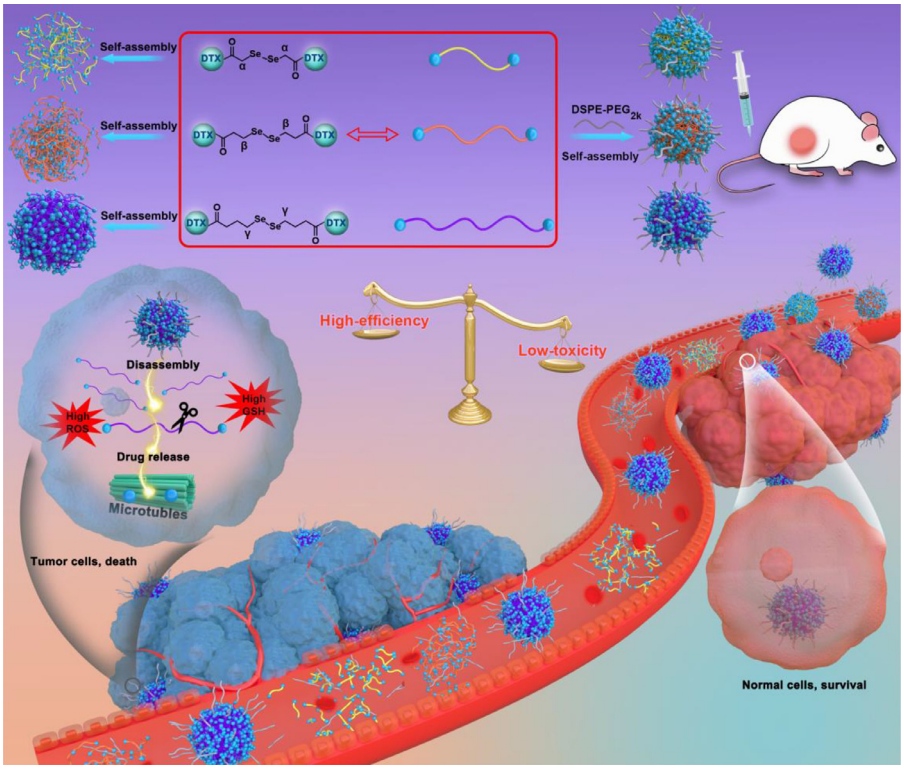

Fig. 1 – Schematic illustration of α-/β-/γ-diselenide bonds-bridged DTX homodimeric prodrug nanoassemblies for efficient chemotherapy.

2′-diselenobisdiglycolic acid, 3, 3′-diselenobisdipropionic acid or 4, 4′-diselenobisdibutyric acid, 0.4 mmol) was added in anhydrous dichloromethane. Then DMAP (9.78 mg, 0.08 mmol) and EDCI (306.72 mg, 1.6 mmol) were added dropwise in above system with stirring for 2 h under nitrogen atmosphere at 25 °C. Then another DMAP (9.78 mg, 0.08 mmol) and EDCI (153.36 mg, 0.8 mmol) were added dropwise for 24 h reaction at 25 °C. Preparative liquid chromatography was utilized to purify the product using acetonitrile/water (70:30) as the mobile phase (yellow solid). Nuclear magnetic resonance spectroscopy (600 MHz ^{1}H NMR, Bruker AV-400) and high-resolution mass spectrometry (Agilent 1100 Series LC/MSD Trap) were applied to confirm the prodrug structure. HPLC was used to identify the purity of the prodrugs.

2.4. *Preparation of DTX homodimeric prodrug nanoassemblies*

One-step nano-precipitation method was used to prepare the DTX homodimeric prodrug nanoassemblies. 4 mg DTX homodimeric prodrugs and 1 mg DSPE-PEG$_{2K}$ were well combined in 1 ml ethanol. Then the mixture ethanol solution was added dropwise into 4 ml deionized water and stirred vigorously to prepare PEGylated DTX homodimeric prodrug nanoassemblies. Ethanol was evaporated by reduced pressure distillation. The non-PEGylated DTX homodimeric prodrug nanoassemblies without the addition of DSPE-PEG$_{2K}$ were prepared by the same procedure. The DiR/coumarin-6-labeled DTX homodimeric prodrug nanoassemblies were formed by co-assembling DTX homodimeric prodrugs with DiR/coumarin-6. Briefly, the mixture of DTX homodimeric prodrugs, DSPE-PEG$_{2K}$ and DiR/coumarin-6 in ethanol were added into deionized water under the vigorously stirring. Zetasizer (Nano ZS, Malvern Co., UK) was applied to measure the Zeta potential and hydrodynamic diameter of DTX homodimeric prodrug nanoassemblies. Transmission electron microscopy (TEM, Hitachi, HT7700, Japan) was applied to determine the morphology of the DTX homodimeric prodrug nanoassemblies.

2.5. *Molecular simulations and colloidal stability*

Three monomer prodrug molecules (α-DSeSeD, β-DSeSeD and γ-DSeSeD) were constructed by Gaussian view 5 software. Based on Gaussian09 program, three monomers were geometric optimized by HF/6–31G* method in PCM recessive solvent model. The bond and dihedral angles of α-/β-/γ-diselenide bond linkages in DTX homodimeric prodrugs were calculated during structure optimization. Molecular docking was applied to predict the molecular interaction via Autodock program, and the binding free energy was obtained. Hydrogen bonding and hydrophobic interactions were analyzed using the Discovery Studio program.

DTX homodimeric prodrug nanoassemblies were incubated in fresh rat plasma at 37 °C for 48 h to evaluate the colloidal stability. The alteration of particle size was analyzed by Zetasizer. In addition, the DTX homodimeric prodrug nanoassemblies were stored at 4 °C for 50 d and 37 °C for 14 d

to test the storage stability. At predetermined time points, the particle size of DTX homodimeric prodrug nanoassemblies was measured.

2.6. *In vitro drug release*

The *in vitro* drug release behavior of DTX homodimeric prodrug nanoassemblies were measured. The pH 7.4 PBS with 30% ethanol (v/v) was used as release media. The DTX homodimeric prodrug nanoassemblies (100 nmol, 0.2 ml) were added in 30 ml release media with or without a series concentration of H_2O_2 and GSH at 37 °C under general shaking. At the predetermined time intervals, a small portion of solution (0.2 ml) was withdrawn from the release medium. HPLC was applied to determine the concentration of DTX released from homodimeric prodrug nanoassemblies ($n = 3$ for each group). To evaluate the redox-responsive drug release mechanism, three homodimeric prodrug nanoassemblies were incubated in 10×10^{-3} M H_2O_2 or 500×10^{-6} M GSH containing release medium at 37 °C under general shaking. The intermediates from prodrugs were confirmed by UPLC-MS-MS (Waters Co., Ltd., Milford, MA, USA).

2.7. *Cell culture*

L02 human normal liver cell line, B16-F10 murine melanoma cell line and 4T1 mouse mammary carcinoma cell line were obtained from the cell bank of Type Culture Collection of Chinese Academy of Sciences (Beijing, China). The 4T1 cells and L02 cells were cultured in Gibco 1640 medium with 10% FBS, streptomycin sulfate (100 μg/ml) and penicillin (100 units/ml). Dulbecco's modified Eagle medium with high-glucose was used to culture the B16-F10 cells. All cells were grown in a 37 °C, 5% CO_2 cell incubator.

2.8. *Cellular uptake*

4T1 cells were placed in 24-well plates (5×10^4 cells/well) for 24 h. After that, the medium was poured, and free coumarin-6 (250 ng/ml) or coumarin-6-labled DTX homodimeric prodrug nanoassemblies (equivalent DTX concentration of 10 μg/ml) in fresh medium was replaced and incubated for 0.5 h or 2 h at 37 °C. Then, cells were washed thrice through cold PBS. 4% formaldehyde was used to fix the cell on the covered lip. After that, cells were washed again, and Hoechst 33 342 was applied to counterstain the nuclei. Confocal laser scanning microscopy (CLSM, TCS SP2/AOBS, LEICA, Germany) was utilized to observe the prepared covered slips. For quantitative analysis, 4T1 cells were placed in 12-well plates (5×10^4 cells/well) for 24 h. Cells were washed thrice, collected and re-suspended in PBS after treated by free coumarin-6 or coumarin-6-labeled DTX homodimeric prodrug nanoassemblies. Cells without treatment were used as control. Flow cytometry was utilized to measure the cellular uptake on a FACS Calibur instrument (Becton Dickinson).

2.9. *Cytotoxicity assays*

The cytotoxicity of DTX homodimeric prodrug nanoassemblies were determined by MTT assays. In brief, B16-F10 cells, 4T1 cells or L02 cells were placed in 96-well plates (1000 cells per well) and incubated for 12 h. After that, the media was poured, and fresh medium containing various predetermined concentrations of Taxotere® or DTX homodimeric prodrug nanoassemblies was further incubated for 48 h ($n = 3$ for each group). Cells without treatment were used as control. Then 35 μl of MTT (5 mg/l) solution was added to plates. After 4 h incubation, the medium in plates were poured and 200 μl dimethyl sulfoxide (DMSO) was added to plates. The absorbance was analyzed using a microplate reader (SYNERGY, BioTek Instruments, Inc, USA) at 490 nm. The calculation of the IC_{50} values were performed using Graph Pad Prism 7. The ratio of the IC_{50} of L02 cell lines to tumor cell lines gained the tumor-selective index (TSI) value.

2.10. *Intracellular drug release*

To evaluate the intracellular drug release, 4T1 cells were placed into 24-well plates (1×10^5 cells/well) for 24 h. After that, the cells were incubated with Taxotere or DTX homodimeric prodrug nanoassemblies (50, 100 and 200 ng/ml, equivalent to DTX) for 48 h. Then, the cells and the culture medium were collected, sonicated and centrifugated. UPLC-MS-MS (ACQUITY UPLCTM, Waters Co., Ltd., Milford, MA, USA) was utilized to determine the concentrations of free DTX in the supernatants.

2.11. *Animal studies*

All the animals were provided by the Laboratory Animal Center of Shenyang Pharmaceutical University (Shenyang, Liaoning, China). All the animal experiments were complied with the Guidelines for the Care and Use of Laboratory Animals and approved by the Institutional Animal Ethical Care Committee (IAEC) of Shenyang Pharmaceutical University.

2.12. *In vivo pharmacokinetic study*

Male Sprague-Dawley rats (180–200 g) were applied to study the pharmacokinetic profiles of DTX homodimeric prodrug nanoassemblies. The animals were intravenously administered Taxotere® or DTX homodimeric prodrug nanoassemblies at a dose equivalent to 4 mg/kg of DTX ($n = 5$ for each group). Blood samples were isolated and centrifuged to obtain the plasma at the predetermined time intervals. UPLC-MS-MS was utilized to analyze the plasma concentration of prodrugs and free DTX. *AUC*, C_{max}, and $T_{1/2}$ were calculated using DAS 2.1.1. The chemical stability of prodrug nanoassemblies in the fresh rat plasma were investigated. At predetermined time intervals, 50 μl samples were withdrawn and 150 μl acetonitrile was added. After vortex and centrifugation, the concentration of the prodrugs and DTX in the supernatants was measured by HPLC.

2.13. *In vivo biodistribution*

Fluorescence imaging was utilized to determine the biodistribution of DTX homodimeric prodrug nanoassemblies. When the tumor volume of 4T1 tumor-bearing BALB/C mice

reached about 400 mm^3, free DiR and DiR-labeled DTX homodimeric prodrug nanoassemblies were administrated at a dose of 1 mg/kg equivalent to DiR via tail vein ($n = 3$ for each group). The mice were sacrificed after 4 h, 12 h and 24 h post injection, and the heart, liver, spleen, lung, kidney and tumor were collected. Noninvasive optical imaging system (IVIS) spectrum small-animal imaging system was used to analyze the fluorescence intensity.

2.14. *In vivo antitumor efficacy*

4T1 cells were subcutaneous injected into the back of female BALB/c mice to establish the tumor model. When the tumor reached about 100 mm^3, the mice were randomly classified into four groups ($n = 5$), and this day was considered as Day 0 for treatment. Then, the mice were intravenously administered saline, Taxotere® or the DTX homodimeric prodrug nanoassemblies (2.5 mg/kg, equivalent to DTX) five injections every other day. The body weight and tumor volume were determined every day. After treatment, the mice were sacrificed, and the tumors were weighed. In addition, the heart, liver, spleen, lung, kidney, and tumor of each group were collected and fixed by formalin for hematoxylin and eosin (H&E) staining. Centrifugation was applied to gain the serum from the collected blood for hepatic and renal function analysis.

To evaluated the tumor accumulation of DTX homodimeric prodrug nanoassemblies, 4T1 tumor-bearing mice were created. When the tumor of mice reached about 400 mm^3, the Taxotere and DTX homodimeric prodrug nanoassemblies were administered at a dose of 10 mg/kg ($n = 3$ for each group) via tail vein. The mice were killed and the tumors were isolated after 4 h, 12 h and 24 h post injection. UPLC-MS-MS was applied to determine the concentrations of prodrugs and DTX at tumor site. TUNEL assay was utilized to evaluate the apoptosis of tumor using an apoptosis detection kit. To determine the proliferation of tumor, Ki-67 immunofluorescence staining was utilized. Nucleus was stained with DAPI, and Olympus IX71 inverted microscope (Japan) was used to observe the processed slides.

2.15. *Statistical analysis*

Analyses were conducted using GraphPad Prism 7.0, and data were calculated as the means ± SD. Statistical comparisons between groups were analyzed with Student's *t*-test (two-tailed). Statistical significance was considered at $^{*}P < 0.05$, $^{**}P < 0.01$, $^{***}P < 0.001$ and $^{****}P < 0.0001$.

3. Results and discussion

3.1. *Synthesis of DTX homodimeric prodrugs*

The synthetic routes of α-DSeSeD, β-DSeSeD and γ-DSeSeD were shown schematically in Fig. S1. The chemical structure of the prodrugs was confirmed by MS and ^{1}H NMR (Fig. S2-S4). The purity of all three prodrugs was over 99% (Fig. S5).

3.2. *Preparation and characterization of prodrug nanoassemblies*

In order to investigate the self-assembly ability of the prodrugs, we first prepared nano-formulations without the addition of any surfactant (Fig. S6). At low concentrations (50 and 100 μg/ml), all three prodrugs could assemble into homogeneous nanoparticles (NPs), and γ-DSeSeD NPs exhibited the minimum particle size with light blue opalescence. At high concentrations (200 and 400 μg/ml), γ-DSeSeD still formed clear and uniform NPs. In comparison, obvious precipitation was observed for α-DSeSeD and β-DSeSeD after centrifugation. These results illustrated that the length of diselenide linkages was one of the most important forces in prodrug self-assembly system and the γ-diselenide bond-containing linkage could facilitate the self-assembly of DTX homodimeric prodrugs.

Since the hydrophobic force is the driver of self-assembly, we first calculated the LogP value of the prodrug, which can reflect the hydrophobicity of the prodrug molecule. As shown in Fig. S7A, the γ-DSeSeD showed the highest LogP value (6.62), followed by β-DSeSeD (6.11) and α-DSeSeD (5.61). This result suggested the γ-DSeSeD have stronger hydrophobic force could form the tightest prodrug nanoassemblies compared to the other prodrugs. However, the over-strong intermolecular force tends to form large drug aggregates. Hence, the role of the diselenide bond-containing linkages in the prodrug self-assembly cannot be ignored. Previous reports have illustrated that the flexibility and self-assembly ability of prodrug was significantly improved by the pivotal linkages, and the approximate 90° bond angle and dihedral angle of linkages exhibited superior ability in self-assembly process [21]. Therefore, we investigated the bond/dihedral angle of diselenide bond in different length linkages (α/β/γ-C-SeSe-C) based on the optimized structure (Fig. 2A). The bond angle and dihedral angle of γ-C-SeSe-C (90.1°/90.5°, 93.6°) were close to 90° compared to β-C-SeSe-C (95.5°/96.9°, 95.6°) and α-C-SeSe-C (97.9°/98.3°, 98.3°). The molecular potential energy of three prodrugs was shown in Fig. S7B. Compared with α-DSeSeD and β-DSeSeD, γ-DSeSeD possessed more flexible molecular potential energy, which could help to balance the force between prodrug molecules. In addition, molecular interaction and binding energy of prodrug nanoassemblies were investigated using molecular docking. As shown in Fig. 2B, the hydrophobic force (pink dashed line) and hydrogen binding (green dashed line) played essential role in self-assembly process. According to thermodynamic aspect, the system releases more energy ($\Delta G < 0$), the more stable structure will be formed. The measured binding energy values were γ-DSeSeD NPs (−410.02 kcal/mol) < β-DSeSeD NPs (−398.54 kcal/mol) < α-DSeSeD NPs (−379.39 kcal/mol), in line with the self-assembly ability of three prodrugs (Fig. 2B). These finding illustrated that the longest γ-diselenide bond-containing linkages possessed the highest flexibility to balance the intermolecular force of DTX homodimeric prodrug, and reduced the total free energy to form more stable prodrug nanoassemblies.

To design prodrug nanoassemblies with high colloidal stability and long half-life, DSPE-PEG_{2K} was co-assembled

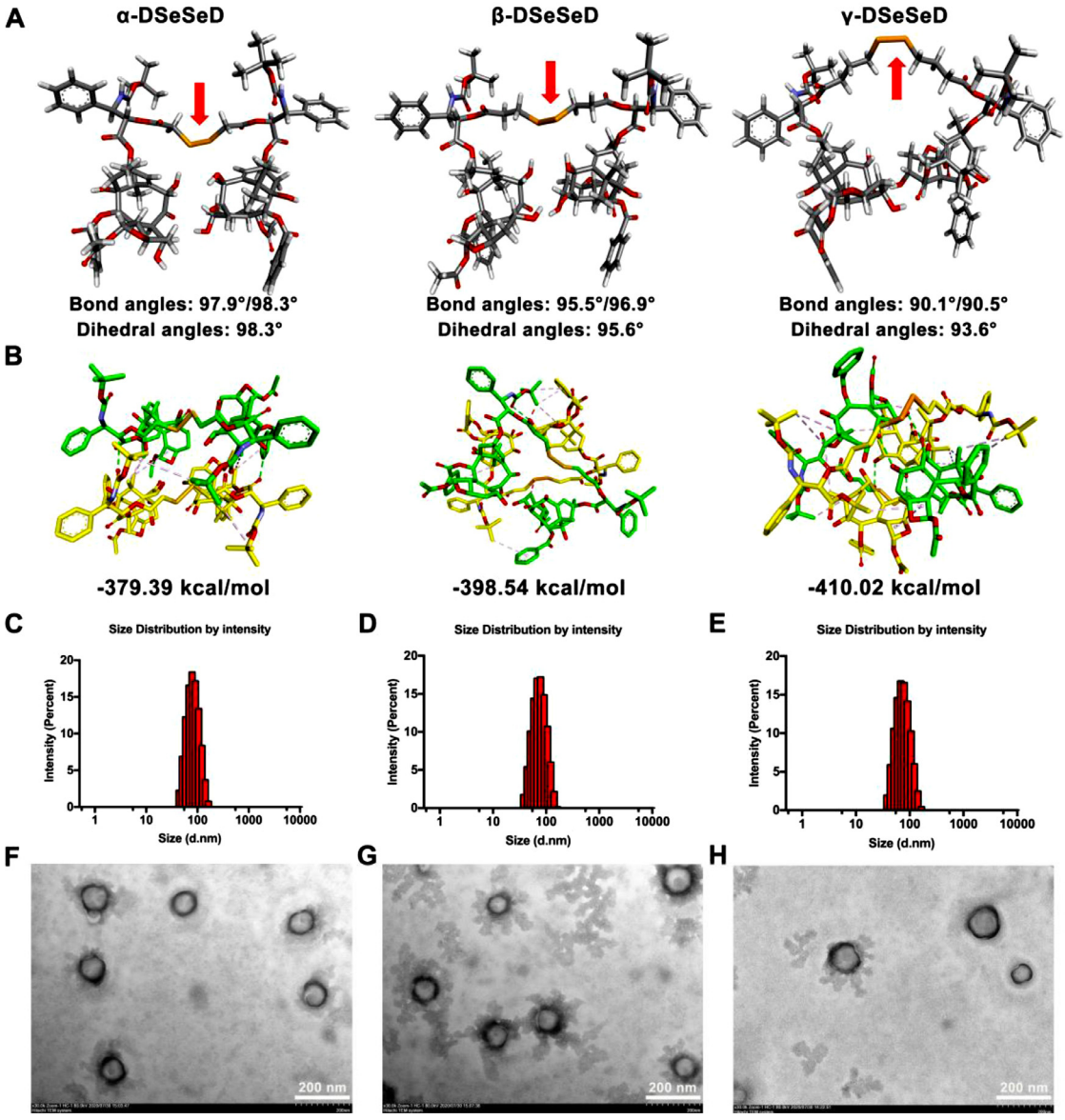

Fig. 2 – Molecular simulations and characterization of prodrug nanoassemblies. (A) The optimized geometry structure and bond/dihedral angles of DTX homodimeric prodrugs. (B) The free binding energy and molecular docking of two prodrug molecules. Particle size distribution of (C) α-DSeSeD NPs, (D) β-DSeSeD NPs and (E) γ-DSeSeD NPs. TEM images of (F) α-DSeSeD NPs, (G) β-DSeSeD NPs and (H) γ-DSeSeD NPs.

with the prodrugs to provide a hydration shell. The prepared NPs showed uniform particle sizes with spherical-shaped structures (Fig. 2C-2H). The hydrodynamic diameter of PEGylated prodrug nanoassemblies was about 80 nm, and the drug loading was approximate 70% (DTX equivalent, w/w) (Table S1). There was no Tween 80 in the preparations, and the only used ethanol was also removed. Therefore, the prodrug nanoassemblies could avoid the hypersensitivity reactions of Taxotere. In addition, all three PEGylated prodrug nanoassemblies were stable under storage condition (Fig. S8), with negligible changes in particle size during 50 d (4 °C) and 14 d (25 °C). As the Taxotere diluent must be used within 6 h in clinic due to its poor stability, the good storage stability of PEGylated prodrug nanoassemblies could facilitate the clinical application of DTX.

The stability of the PEGylated prodrug nanoassemblies were further assessed in the fresh rat plasma (Fig. S9). γ-DSeSeD NPs remained uniform and stable within 48 h. In comparison, there was a sharp rise in the particle size of α-DSeSeD NPs and β-DSeSeD NPs. This suggested that PEG-modification could enhance the stability of prodrug nanoassemblies to some extent, but was unable to alter the impacts of linkages. The γ-diselenide bond-bridged DTX homodimeric prodrug nanoassemblies possessed superior stability, which may contribute to the *in vivo* pharmacokinetics.

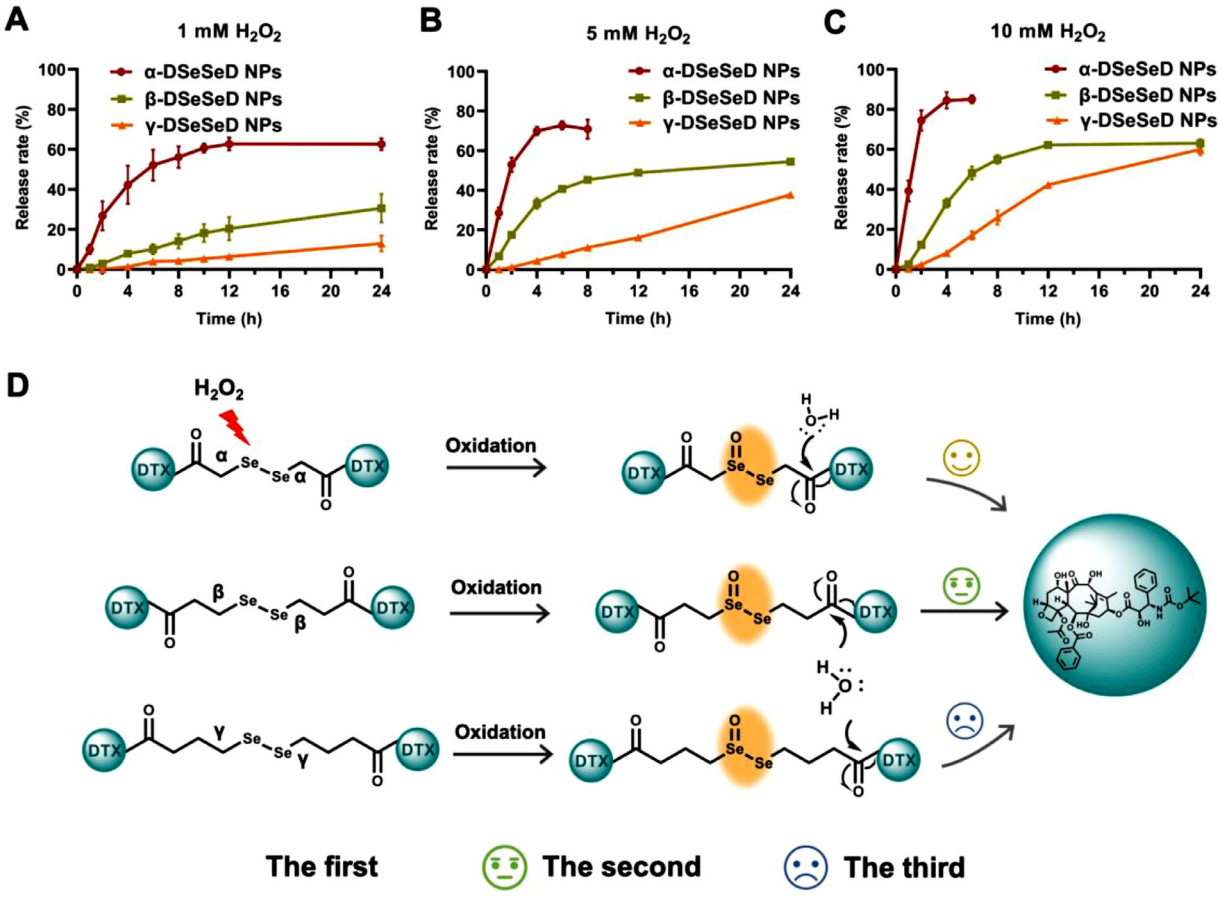

Fig. 3 – Oxidation-responsive drug release of DTX homodimeric prodrug nanoassemblies in (A) 1 mM H_2O_2, (B) 5 mM H_2O_2 and (C) 10 mM H_2O_2. (D) Oxidation-responsive mechanism of α-diselenide bond, β-diselenide bond and γ-diselenide. Data are presented as the mean ± SD ($n = 3$).

3.3. *Redox-triggered drug release*

In blank media, the proportion of DTX released from γ-DSeSeD NPs, β-DSeSeD NPs and α-DSeSeD NPs was 1.04%, 11.39% and 24.25%, respectively (Fig. S10). These finding suggested that γ-diselenide bond-containing linkage was able to reduce the premature drug leakage in systemic circulation and thus alleviate the undesired toxicity of DTX, which could be ascribed to the enhanced stability of γ-DSeSeD NPs.

Due to the redox dual-responsivity of diselenide bond, the difference in drug release among these three prodrug nanoassemblies were investigated in detail. H_2O_2 and GSH were used as model triggers. The release rate of DTX was proportional to the concentration of H_2O_2, following the order of α-DSeSeD NPs > β-DSeSeD NPs > γ-DSeSeD NPs (Fig. 3A-3C). In the present of H_2O_2, the selenium atoms were oxidized to hydrophilic selenoxide, then promoting the hydrolysis of DTX-linked eater bond (Fig. 3D). As a result, the release rate of DTX was directly based on the distance between the selenium atom and the easter bond, and α-diselenide bond showed the faster drug release profile due to the shortest distance. In order to confirm the release mechanism, the prodrug nanoassemblies were incubated with 10 mM H_2O_2, and the molecular weights of the midbody were measured by mass spectrometry (Fig. S11). The mass spectra of α-DSeSeD (1896), β-DSeSeD (1924) and γ-DSeSeD (1951) illustrated the formation of selenoxide ($[M_{monoxide}+Na]^+$).

Additionally, we further evaluated the reduction-responsivity of DTX homodimeric prodrug nanoassemblies (Fig. 4A-4C). γ-DSeSeD NPs showed increased DTX release with the increasing of the concentration of GSH, and could release approximate 80% of the DTX after incubating with 5 mM GSH for 24 h. Interestingly, the DTX release of α-DSeSeD NPs was similar at low GSH concentration (5–500 μM), but significantly reduced at high GSH concentration (5000 μM). As for β-DSeSeD NPs, the percentage of DTX release was extremely low (less than 10%) regardless of the concentration of GSH (5–5000 μM). The mechanism of drug release was illustrated in Fig. 4D. Firstly, the diselenide bond was attacked by nucleophilic GSH, resulting in the formation of DSe-SG and DSe-H (Fig. S12-S14). After that, the DSe-H had two possible changes based on its stability: one was to promote the hydrolysis of the DTX-linked ester bond, the other was attacked by excess GSH to generate new DSe-SG. As the drug release rate (or the hydrolysis of ester bond) was depended on the distance between the selenol and the ester bond, α-DSe-H showed much quicker drug release rate than β-DSe-H. However, the excess GSH also tended to attack α/β-DSe-H to generate new α/β-DSe-SG and

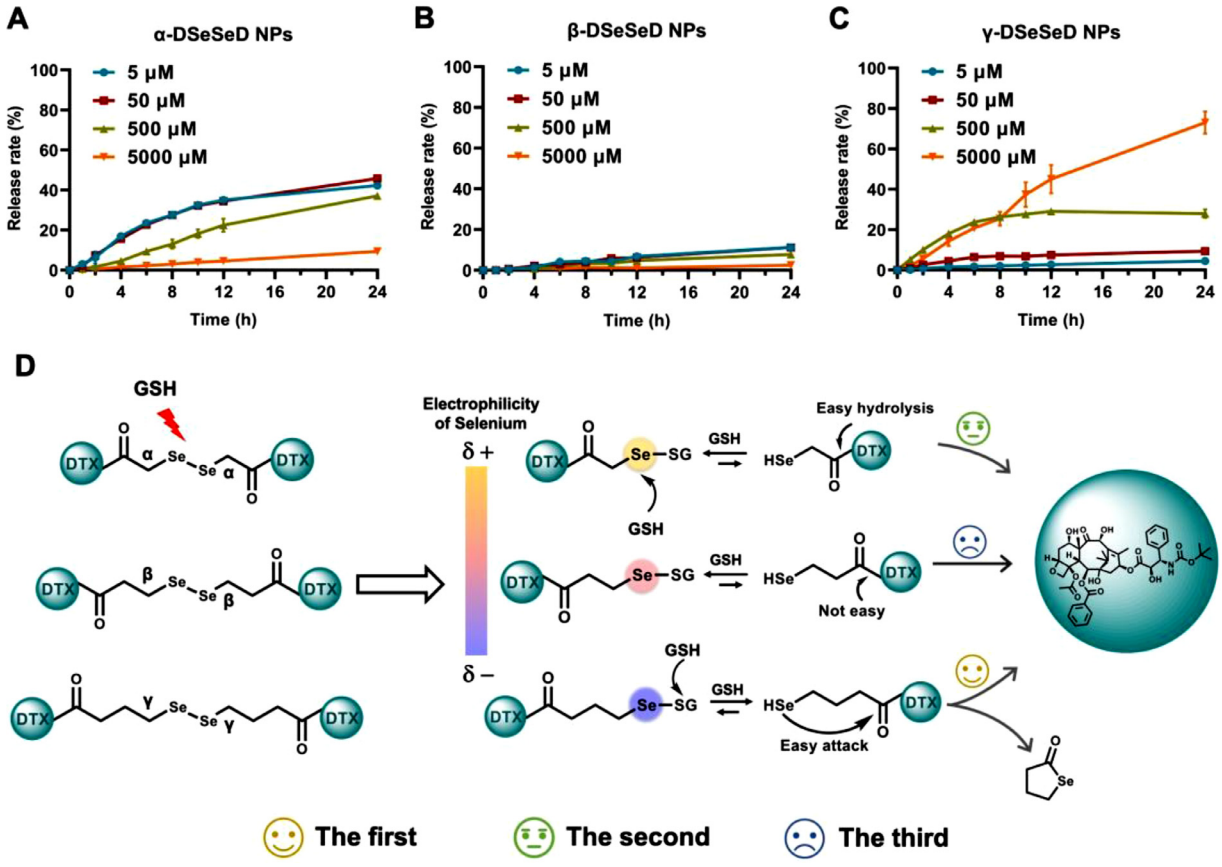

Fig. 4 – Reduction-triggered drug release of (A) α-DSeSeD NPs, (B) β-DSeSeD NPs and (C) γ-DSeSeD NPs. (D) Reduction-responsive mechanism of α-diselenide bond, β-diselenide bond and γ-diselenide. Data are presented as the mean ± SD ($n = 3$).

then prevent the release of DTX. Therefore, α-DSeSeD NPs and β-DSeSeD NPs showed extremely low release rate at high concentration of GSH. In comparison, γ-DSe-H could avoid the attack of GSH because the selenol with suitable length was more tended to attack the DTX-linked ester bond, leading to the generation of stable five-membered ring and the release of DTX.

On the other hand, GSH could also attack the Se or S of DSe-SG, along with the generation of DSe-SG (invalid for drug release) and DSe-H (effective for drug release), respectively. In general, GSH prefer to react with the electrophilic Se because the electron pair of Se-S bond is farther from Se. In this sense, the electrophilicity of selenium atoms in DSe-SG determines the direction of reaction. The electron cloud density of selenium atom in DSe-SG was also affected by the adjacent electro-withdrawing group (-COOR). Therefore, the degree of the electrophilicity of selenium atom followed the order of α-DSe-SG > β-DSe-SG > γ-DSe-SG, which is depended on the distance between the selenium atom and the electro-withdrawing group (-COOR). Hence, the additional GSH tended to react with the more electrophilic Se of α-DSe-SG, thus formed the other α-DSe-SG (invalid for drug release). In comparison, γ-DSe-SG weakened this tendency, and had more possibility to form γ-DSe-H (effective for drug release) rather than γ-DSe-SG. These results illustrated that the length of diselenide bond-containing linkages affected not only the release rate but also the release mechanism of homodimeric prodrug nanoassemblies.

As shown in Fig. 3A-3C and Fig. 4A-4C, the amount of the maximal DTX released from prodrugs were less than 80% in the presence of H_2O_2 and GSH. One explanation might be that the DTX was degraded in the present of H_2O_2. In addition, there are several intermediates after the nucleophilic attack by GSH as our above mentioned.

3.4. *Cellular uptake*

We next determined the cellular uptake of DTX homodimeric prodrug nanoassemblies. In comparison to control group, prodrug nanoassemblies-treated groups possessed extremely stronger intracellular fluorescence intensity (Fig. 5A–5D). In addition, these three prodrug nanoassemblies displayed similar cellular uptake behavior, since they have similar size and morphology. α-DSeSeD NPs-treated cells showed slightly stronger fluorescence intensity than another two groups (Fig. 5C). This was because the fast disassembly of α-DSeSeD NPs recovering the fluorescence intensity of coumarin-6, which was quenched in prodrug nanoassemblies due to aggregation-caused quenching (ACQ) effect. This result was further proved by intercellular drug release subsequently.

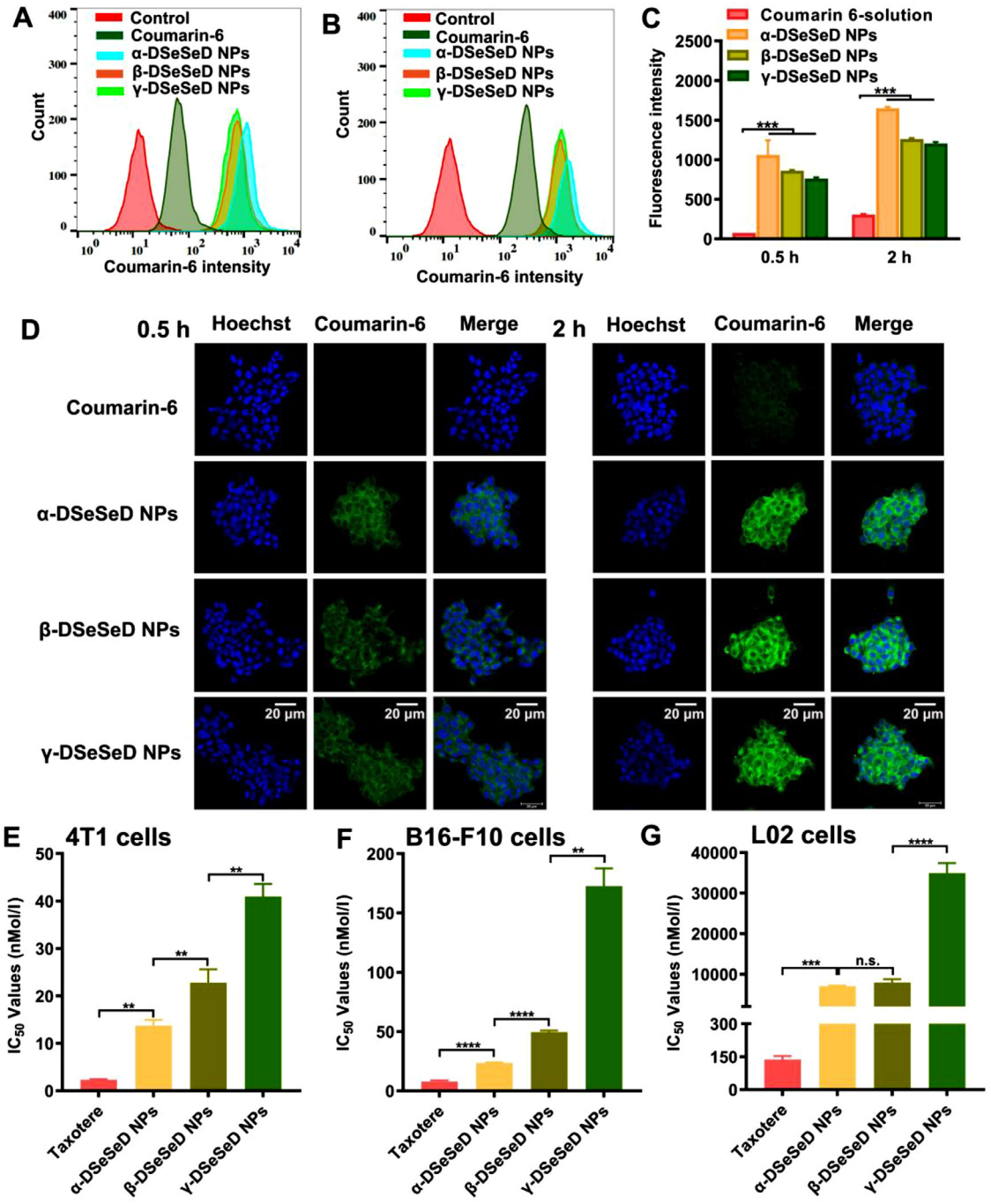

Fig. 5 – Cytotoxicity and cellular uptake. Flow cytometry measurements of 4T1 cells treated with coumarin-6 solution or coumarin-6-loaded DTX homodimeric prodrug nanoassemblies at 0.5 h (A) and (B) 2 h. (C) Fluorescence intensity of flow cytometry analysis. (D) CLSM images at 0.5 h and 2 h. Scale bar represents 20 μm. IC_{50} values of Taxotere and DTX homodimeric prodrug nanoassemblies on (E) 4T1 cells, (F) B16-F10 cells and (G) L02 cells. Data are presented as mean ± SD ($n = 3$).

3.5. *Cytotoxicity*

As shown in Fig. 5E-5F & S15 and Table S2, DTX homodimeric prodrug nanoassemblies displayed lower cytotoxicity than Taxotere in tumor cells, following the order of Taxotere® > α-DSeSeD NPs > β-DSeSeD NPs > γ-DSeSeD NPs. We speculated the cytotoxicity was depended on the release rate of active drug from prodrug nanoassemblies. Therefore, the intracellular drug release rate of DTX homodimeric prodrug nanoassemblies was further investigated in 4T1 cells (Fig. S16). The amount of DTX release from α-DSeSeD NPs was higher than that from β-DSeSeD NPs and γ-DSeSeD NPs after incubated with 4T1 cells for 48 h, agreeing well with the cellular uptake and cytotoxicity results. These finding

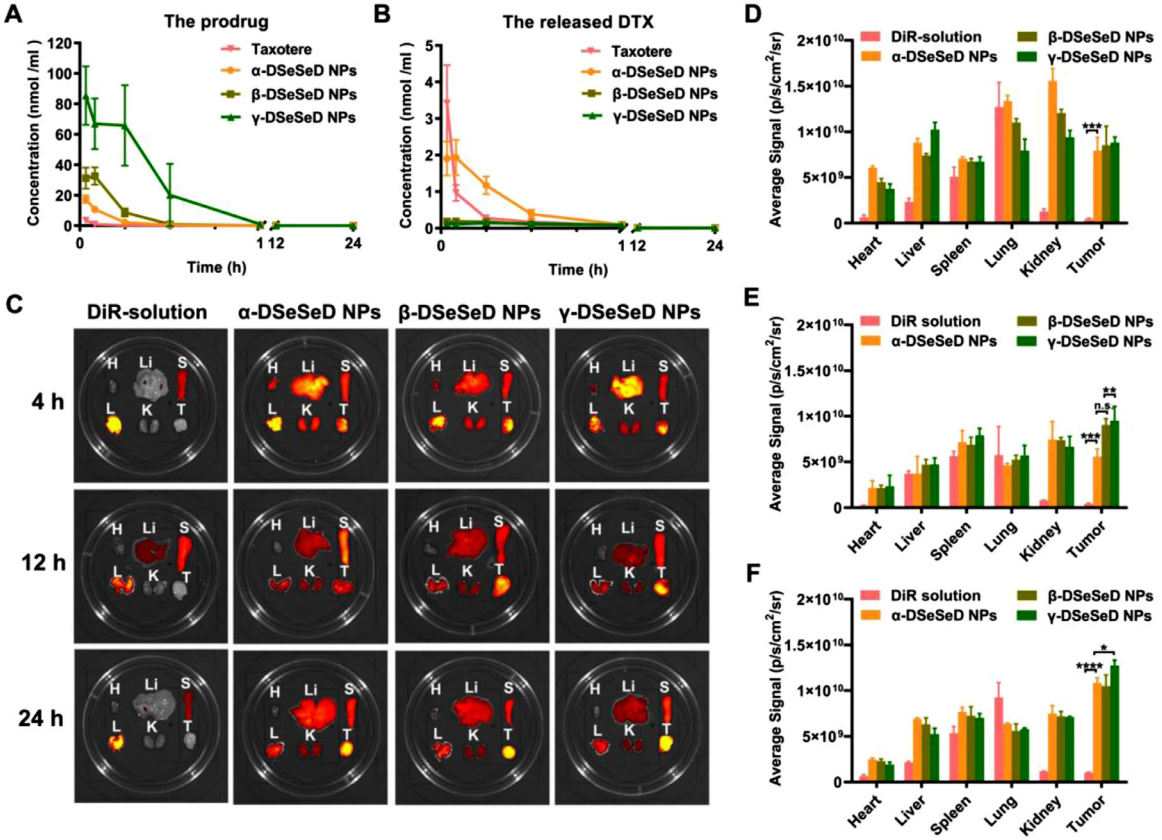

Fig. 6 – *In vivo* pharmacokinetics and biodistribution. Molar concentration-time curves of the (A) prodrugs and (B) the released DTX. Data are presented as the mean ± SD ($n = 5$). (C) Fluorescent imaging of DiR or DiR-labeled prodrug nanoassemblies in tumors and main organs. Quantitative analysis of fluorescent signals in tumors and main organs at (D) 4 h, (E) 12 h and (F) 24 h. Data are presented as mean ± SD ($n = 3$).

suggested that cytotoxicity of DTX homodimeric prodrug nanoassemblies was closely related to the drug release rate: faster release rate resulted in higher cytotoxicity.

In addition, prodrug nanoassemblies possessed lower cytotoxicity than Taxotere on L02 cells (Fig. 5G). The tumor-selective index (TSI) of Taxotere and prodrug nanoassemblies was summarized in Table S3. Three prodrug nanoassemblies showed much higher TSI values than Taxotere, which means the high tumor selectivity of prodrug nanoassemblies. It is well known that the redox state of tumor cells is much higher than normal cells [21]. These results indicated that prodrug nanoassemblies were able to selectively kill tumor cells due to redox-triggered release of DTX, showing good safety in the normal cells.

3.6. *In vivo pharmacokinetics and biodistribution*

As shown in Fig. 6A-6B, DTX in Taxotere was rapidly cleared from blood circulation. In comparison, prodrug nanoassemblies could dramatically prolong the blood circulation time of DTX. Moreover, the *AUC* of total DTX (the released DTX plus the prodrug) in the α-DSeSeD NPs, β-DSeSeD NPs and γ-DSeSeD NPs groups were approximately 6.8-, 11.9- and 46.4-times higher than Taxotere group, respectively (Table S4). These finding suggested that the length of diselenide bond-containing linkages impacted the pharmacokinetic profiles of prodrug nanoassemblies. Among three NPs, the γ-DSeSeD NPs exhibited the longest blood circulation and highest *AUC*, probably because of the enhanced colloidal stability. Additionally, the *AUC* of the released DTX followed the sequence of α-DSeSeD NPs > β-DSeSeD NPs > γ-DSeSeD NPs, agreeing well with the drug release in blank medium. Furthermore, the chemical stability of prodrug nanoassemblies was assessed in the fresh rat plasma (Fig. S17). The γ-DSeSeD NPs possessed good chemical stability, with approximately 80% of the prodrug remained intact in the fresh rat plasma within 24 h. However, the α-DSeSeD NPs showed poor chemical stability, which only kept 10% prodrugs after 24 h incubation. These results confirmed that both colloidal stability and chemical stability had great impacts on their pharmacokinetic behavior of prodrug nanoassemblies. γ-diselenide bonds-containing linkage in prodrug structure played a key role in improving the pharmacokinetics of DTX homodimeric prodrug nanoassemblies.

Fluorescence imaging was applied to study the biodistribution of DTX homodimeric prodrug nanoassemblies (Fig. 6C–6F). Free DiR solution exhibited high fluorescent signal in spleens, lungs and livers, but negligible fluorescent signal was observed in tumors. Compared to free DiR

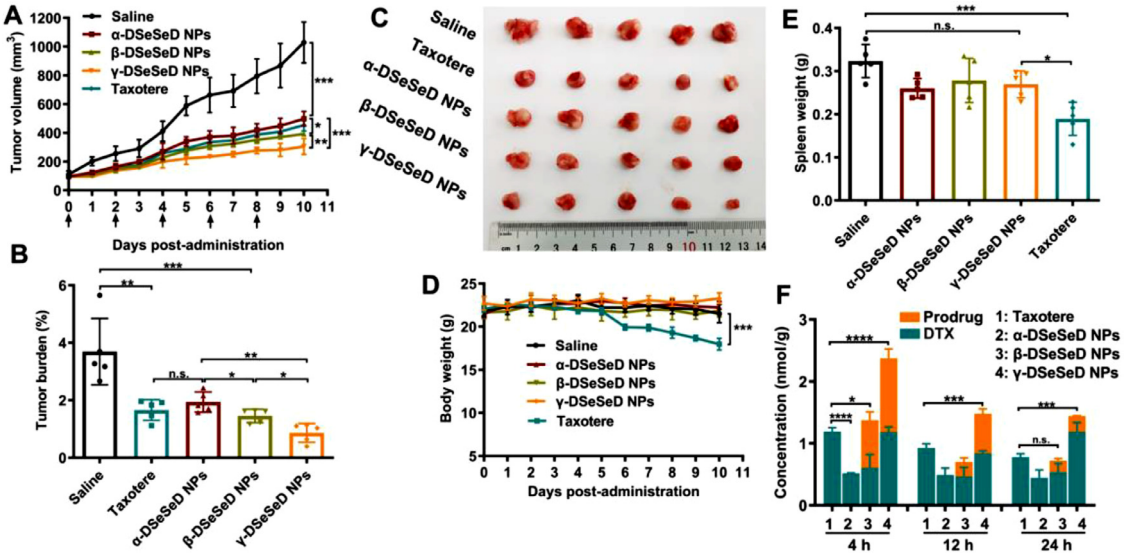

Fig. 7 – *In vivo* antitumor efficacy of Taxotere and prodrug nanoassemblies against 4T1 tumors. (A) Tumor volume. (B) Tumor burden. (C) Images of tumors. (D) Body weight changes. (E) Spleen weight. Data are presented as the mean ± SD ($n = 5$). (F) Tumor accumulation of Taxotere and DTX homodimeric prodrug nanoassemblies. Data are presented as the mean ± SD ($n = 3$).

solution, the fluorescent intensity of DiR-labeled DTX homodimeric prodrug nanoassemblies were dramatically increased in tumor sections from 4 h to 24 h. The long blood circulation time of prodrug nanoassemblies contributed to their improved tumor accumulation. Therefore, γ-DSeSeD NPs with good stability showed higher tumor accumulation than α-DSeSeD NPs and β-DSeSeD NPs.

3.7. *In vivo antitumor efficacy*

We further determine the impacts of linkages on the antitumor activity of prodrug nanoassemblies. The tumor burden and tumor volume of Taxotere-treated mice was between that of α-DSeSeD NPs and β-DSeSeD NPs-treated groups, and there was no significant difference between Taxotere and each of them (Fig. 7A-7C). In addition, β-DSeSeD NPs and γ-DSeSeD NPs showed better antitumor efficacy than α-DSeSeD NPs. Although the α-DSeSeD NPs exhibited the fastest intracellular drug release and strongest cytotoxicity, the rapid systemic clearance and limited tumor accumulation restricted their antitumor activity. Interestingly, γ-DSeSeD NPs exhibited the best antitumor activity, despite γ-DSeSeD NPs showed the lowest cytotoxicity in 4T1 cells. These finding illustrated that the antitumor efficacy of DTX homodimeric prodrug nanoassemblies was the integration of colloidal and chemical stability, pharmacokinetics, tumor accumulation, and tumor-specific drug release. We propose that the *in vivo* antitumor efficacy was ultimately depended on the concentration of active DTX in tumor sites, which could really reflect the efficiency of drug delivery. Therefore, we further studied the tumor accumulation of Taxotere and prodrug nanoassemblies using UPLC-MS-MS (Fig. 7F). The γ-DSeSeD NPs displayed more tumor accumulation (both DTX and prodrug) than other groups, which was consistent with the colloidal stability, chemical stability and the *in vivo* pharmacokinetic abovementioned. Although γ-DSeSeD NPs exhibited relative low cytotoxicity to 4T1 cells, their stable nanostructure remained intact in the blood circulation and had the effective potential to reach tumor, and then specifically released active DTX in tumor cell, which finally "turned the table". Hence, small changes in the length of diselenide bond-containing linkages exert great influences on the antitumor activity of DTX homodimeric prodrug nanoassemblies.

TUNEL assays was used to investigate the cellular apoptosis of tumor sections. γ-DSeSeD NPs caused much more cellular apoptosis than other groups (Fig. S18A). Furthermore, prodrug nanoassemblies, especially γ-DSeSeD NPs, significantly reduced the level of Ki-67 in tumor tissues (Fig. S18B).

The body weight of Taxotere-treated mice significantly decreased after the treatment, while there was no change in prodrug nanoassemblies-treated groups (Fig. 7D). In addition, Taxotere led to hepatic function damage since the ALT and AST values were reduced compared with saline group (Fig. S19). In the complete blood test, there were no differences between the saline group and prodrug nanoassemblies (Fig. S20). H&E stain tissue sections of major organ were summarized in Fig. S21. A widespread pyknosis and karyorrhexis of liver cells were observed in Taxotere-treated group, which means the incidence of necrosis. Besides, the spleen of Taxotere-treated group was shrunk, indicating the occurrence of myelosuppression (Fig. 7E). These results revealed that Taxotere caused severe adverse side effects. In comparison, prodrug nanoassemblies exhibited good safety with no body weights changes and negligible systemic toxicity, alleviating the nonspecific toxicity of DTX.

4. Conclusion

In this study, we designed three DTX homodimeric prodrugs with various lengths of diselenide bond-containing linkages. These prodrugs were able to form homogeneous NPs with approximate 70% drug loading. The influence of these diselenide bonds on the antitumor activity of DTX homodimeric prodrug nanoassemblies were deeply investigated. Compared with α- and β-diselenide bonds, γ-diselenide bond-containing linkage could improve the self-assembly of DTX homodimeric prodrugs, thus showed distinct superiority in colloidal stability, circulation time and tumor accumulation. The length of linkages also affected the redox-triggered drug release, thereby impacted the cytotoxicity of prodrug nanoassemblies. Although γ-DSeSeD NPs exhibited the lowest cytotoxicity to 4T1 cells, the stable γ-DSeSeD NPs maintained intact during circulation and achieved the maximum accumulation of DTX in tumor cells, which finally "turned the table". Our work illustrated the pivotal role of linkages on the homodimeric prodrug nanoassemblies, and provided new insights into the rational design of advanced nanomedicine.

Conflicts of interest

The authors report no conflicts of interest. The authors alone are responsible for the content and writing of this article.

Acknowledgments

This work was supported by China Postdoctoral Innovative Talents Support Program (no. BX20190219), China Postdoctoral Science Foundation (no. 2019M661134), and National Natural Science Foundation of China (no. 81872816).

Supplementary materials

Supplementary material associated with this article can be found, in the online version, at doi:10.1016/j.ajps.2021.02.002.

REFERENCES

[1] Hellmann M, Li B, Chaft J, Kris M. Chemotherapy remains an essential element of personalized care for persons with lung cancers. Ann Oncol 2016;27(10):1829–35.
[2] Perou CM, Sørlie T, Eisen MB, van de Rijn M, Jeffrey SS, Rees CA, et al. Molecular portraits of human breast tumours. Nature 2000;406(6797):747–52.
[3] Hayashi N, Yagata H, Tsugawa K, Kajiura Y, Yoshida A, Takei J, et al. Response and prognosis of docetaxel and cyclophosphamide as neoadjuvant chemotherapy in ER(+) HER2(-) breast cancer: a prospective phase II study. Clin Breast Cancer 2020.
[4] Batra A, Hannouf MB, Alsafar N, Lupichuk S. Four cycles of docetaxel and cyclophosphamide as adjuvant chemotherapy in node negative breast cancer: a real-world study. Breast 2020;54:1–7.
[5] Santonja A, Sánchez-Muñoz A, Lluch A, Chica-Parrado MR, Albanell J, Chacón JI, et al. Triple negative breast cancer subtypes and pathologic complete response rate to neoadjuvant chemotherapy. Oncotarget 2018;9(41):26406–16.
[6] Abdel-Rahman O. Efficacy and toxicity outcomes of elderly castrate-resistant prostate cancer patients treated with docetaxel-A pooled analysis of 3 randomized studies. Urol Oncol 2020;38(4):210–15.
[7] Al-Batran SE, Hozaeel W, Tauchert FK, Hofheinz RD, Hinke A, Windemuth-Kieselbach C, et al. The impact of docetaxel-related toxicities on health-related quality of life in patients with metastatic cancer (QoliTax). Ann Oncol 2015;26(6):1244–8.
[8] Aires Fernandes MO, Eloy J, Tavares Luiz M, Ramos Junior SL, Borges JC, Rodríguez de la Fuente L, et al. Transferrin-functionalized liposomes for docetaxel delivery to prostate cancer cells. Colloids Surf A 2021;611:125806.
[9] Liang C, Bai X, Qi C, Sun Q, Han X, Lan T, et al. Pi electron-stabilized polymeric micelles potentiate docetaxel therapy in advanced-stage gastrointestinal cancer. Biomaterials 2021;266:120432.
[10] Luo C, Sun J, Sun B, He Z. Prodrug-based nanoparticulate drug delivery strategies for cancer therapy. Trends Pharmacol Sci 2014;35(11):556–66.
[11] Walther R, Rautio J, Zelikin AN. Prodrugs in medicinal chemistry and enzyme prodrug therapies. Adv Drug Deliv Rev 2017;118:65–77.
[12] Sharma A, Lee MG, Won M, Koo S, Arambula JF, Sessler JL, et al. Targeting heterogeneous tumors using a multifunctional molecular prodrug. J Am Chem Soc 2019;141(39):15611–18.
[13] Hartshorn CM, Bradbury MS, Lanza GM, Nel AE, Rao J, Wang AZ, et al. Nanotechnology strategies to advance outcomes in clinical cancer care. ACS Nano 2018;12(1):24–43.
[14] Shi J, Kantoff PW, Wooster R, Farokhzad OC. Cancer nanomedicine: progress, challenges and opportunities. Nat Rev Cancer 2017;17(1):20–37.
[15] van der Meel R, Sulheim E, Shi Y, Kiessling F, Mulder WJM, Lammers T. Smart cancer nanomedicine. Nat Nanotechnol 2019;14(11):1007–17.
[16] Peng Y, Chen L, Ye S, Kang Y, Liu J, Zeng S, et al. Research and development of drug delivery systems based on drug transporter and nano-formulation. Asian J Pharm Sci 2020;15(2):220–36.
[17] Zhang X, Zhang T, Ma X, Wang Y, Lu Y, Jia D, et al. The design and synthesis of dextran-doxorubicin prodrug-based pH-sensitive drug delivery system for improving chemotherapy efficacy. Asian J Pharm Sci 2020;15(5):605–16.
[18] Sun B, Luo C, Cui W, Sun J, He Z. Chemotherapy agent-unsaturated fatty acid prodrugs and prodrug-nanoplatforms for cancer chemotherapy. J Control Release 2017;264:145–59.
[19] Sun B, Luo C, Zhang X, Guo M, Sun M, Yu H, et al. Probing the impact of sulfur/selenium/carbon linkages on prodrug nanoassemblies for cancer therapy. Nat Commun 2019;10(1):3211.
[20] Zuo S, Sun B, Yang Y, Zhou S, Zhang Y, Guo M, et al. Probing the superiority of diselenium bond on docetaxel dimeric prodrug nanoassemblies: small roles taking big responsibilities. Small 2020;16(45):e2005039.
[21] Yang Y, Sun B, Zuo S, Li X, Zhou S, Li L, et al. Trisulfide bond–mediated doxorubicin dimeric prodrug nanoassemblies with high drug loading, high self-assembly stability, and high tumor selectivity. Sci Adv 2020;6:eabc1725.
[22] Sun B, Chen Y, Yu H, Wang C, Zhang X, Zhao H, et al. Photodynamic PEG-coated ROS-sensitive prodrug nanoassemblies for core-shell synergistic

chemo-photodynamic therapy. Acta Biomater 2019;92:219–28.
[23] Li T, Xu H. Selenium-containing nanomaterials for cancer treatment. Cell Reports Physical Science 2020;1(7):1–7.
[24] Ma N, Li Y, Xu H, Wang Z, Zhang X. Dual redox responsive assemblies formed from diselenide block copolymers. J Am Chem Soc 2010;132(2):442–3.
[25] Sun C, Wang L, Xianyu B, Li T, Gao S, Xu H. Selenoxide elimination manipulate the oxidative stress to improve the antitumor efficacy. Biomaterials 2019;225:119514.
[26] Chuard N, Poblador-Bahamonde AI, Zong L, Bartolami E, Hildebrandt J, Weigand W, et al. Diselenolane-mediated cellular uptake. Chem Sci 2018;9(7):1860–6.
[27] Qiu L, Ge L, Long M, Mao J, Ahmed KS, Shan X, et al. Redox-responsive biocompatible nanocarriers based on novel heparosan polysaccharides for intracellular anticancer drug delivery. Asian J Pharm Sci 2020;15(1):83–94.
[28] Gao S, Li T, Guo Y, Sun C, Xianyu B, Xu H. Selenium-containing nanoparticles combine the NK cells mediated immunotherapy with radiotherapy and chemotherapy. Adv Mater 2020;32(12):e1907568.
[29] Yin W, Ke W, Lu N, Wang Y, Japir A, Mohammed F, et al. Glutathione and reactive oxygen species dual-responsive block copolymer prodrugs for boosting tumor site-specific drug release and enhanced antitumor efficacy. Biomacromolecules 2020;21(2):921–9.
[30] Sun B, Luo C, Yu H, Zhang X, Chen Q, Yang W, et al. Disulfide bond-driven oxidation- and reduction-responsive prodrug nanoassemblies for cancer therapy. Nano Lett 2018;18(6):3643–50.
[31] Li S, Shan X, Wang Y, Chen Q, Sun J, He Z, et al. Dimeric prodrug-based nanomedicines for cancer therapy. J Control Release 2020;326:510–22.
[32] Cai K, He X, Song Z, Yin Q, Zhang Y, Uckun FM, et al. Dimeric drug polymeric nanoparticles with exceptionally high drug loading and quantitative loading efficiency. J Am Chem Soc 2015;137(10):3458–61.
[33] Pei Q, Hu X, Liu S, Li Y, Xie Z, Jing X. Paclitaxel dimers assembling nanomedicines for treatment of cervix carcinoma. J Control Release 2017;254:23–33.